

# CloudWalker: 3D Point Cloud Learning by Random Walks for Shape Analysis

Adi Mesika

Technion Israel Institute of Technology

sadim@campus.technion.ac.il

Yizhak Ben-Shabat

Technion Israel Institute of Technology and

Australian National University

sitzikbs@technion.ac.il

Ayellet Tal

Technion Israel Institute of Technology

ayellet@ee.technion.ac.il

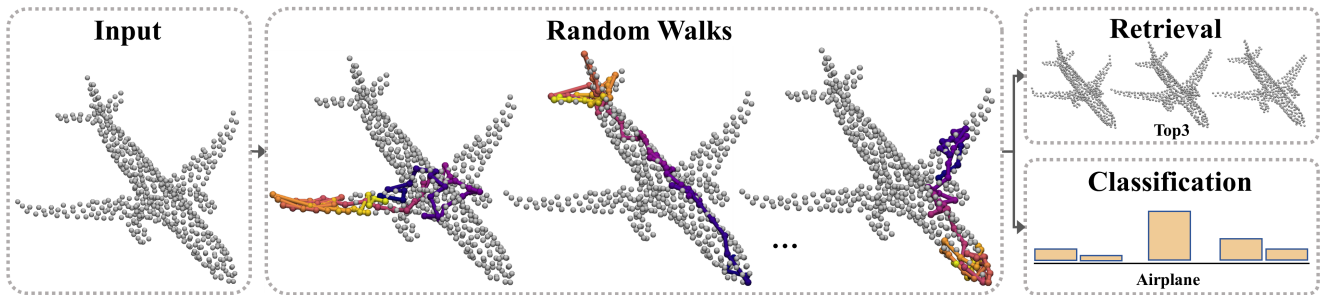


Figure 1. **CloudWalker’s pipeline.** A set of random walks is generated for a given point cloud. Each walk explores the object on its path (points on the walk are color-coded according to their position in the walk sequence, from blue to yellow). We use CloudWalker for two tasks: 3D object retrieval and classification and achieve state of the art results.

## Abstract

Point clouds are gaining prominence as a method for representing 3D shapes, but its irregular structure poses a challenge for deep learning methods. In this paper we propose *CloudWalker*, a novel method for learning 3D shapes using random walks. Previous works attempt to adapt Convolutional Neural Networks (CNNs) or impose a grid or mesh structure to 3D point clouds. This work presents a different approach to represent and learn the shape from a given point set. The key idea is to impose structure on the point set by multiple random walks through the cloud for exploring different regions of the 3D object. Then we learn a per-point and per-walk representation and aggregate multiple walk predictions at inference. Our approach achieves state-of-the-art results for two 3D shape analysis tasks: classification and retrieval. Furthermore, we propose a shape complexity indicator function that uses cross-walk and inter-walk variance measures to subdivide the shape space.

## 1. Introduction

Three dimensional data acquired by sensors provides rich geometric information. Various formats are used to represent this data, including multi-view images, volumetric grids, meshes, implicit functions and point clouds [8, 11, 20]. Our focus is on point cloud representation, which is a sampling of a continuous surface. It is often the rawest form of data obtained by modern 3D scanners.

Point clouds manage to preserve the original geometric information in 3D space without the need of discretization. However, there are challenges associated with this representation, particularly in the context of deep learning approaches. These include the lack of connectivity information, the lack of structure and order, the varied number of points, and corruptions in the form of noise, incompleteness, and density variations. An additional difficulty is the lack of large-scale datasets.

Several approaches have been recently proposed for point cloud deep learning. Point-wise *Multilayer perceptron (MLP)* methods explored global/local structures to enhance feature learning and overcome the permutation variance (order) using a symmetric function [23, 24, 37]. Oth-

ers propose convolutional-based methods, which can be divided into continuous [18, 19, 30, 33, 36] and discrete [17, 27]. These methods overcome some of the structural challenges using local connectivity information. Some works consider each point as a vertex of the graph, by adding edges that connect points, and apply graph networks [28]. Finally, others are constructed based on different hierarchical data structures (e.g., Octree and KD-tree) [13, 15]. While all of the above works handle the challenges of lack of structure and order, none has shown to be as effective as CNNs are for images. Therefore, the challenge of learning a representation for point clouds remains an active field of research.

Our work takes a different avenue. We propose to represent a point cloud by random walks through the cloud, which "explore" the shape. Intuitively, such a walk moves from point to point, through the cloud's valleys and ridges, and on its way discovers the geometry of the underlying surface. A walk is essentially a sequence of points. In a way, this sequence imposes some structure, which is essential for deep learning. A point cloud is represented by multiple walks, which partially cover the underlying surface. Due to their randomness, some walks provide a more global view of the object, whereas others are local and focus on specific parts.

In recent years, random walks have been used for a variety of 3D model representations. Some methods use walks on graphs [22] or on meshes [14]. In [35] it is proposed to use guided walks for point clouds. They generate walks based on a given set of rules and heuristics. We, however, utilize the power of randomness and show that we achieve good results despite the simplicity of our approach.

We show how to handle some challenges: First, we address the generation of walks despite the lack of connectivity information. We show how to do that efficiently. Furthermore, unlike some previous algorithms [23, 24, 36], our approach does not require normal vectors as inputs to improve performance. This is an important property since normal estimation is particularly inaccurate for noisy real-world point clouds [1, 10, 16].

Our approach is general in the sense that it can be used for various shape analysis tasks. We demonstrate its performance on two tasks: 3D object classification and 3D object retrieval. Our results are compared against the reported SOTA results for commonly-used datasets *3D-Future* [9], *ScanObjectNN* [2, 31], and *ModelNet40* [34].

This paper makes three main contributions:

- We propose a novel representation for point cloud shape analysis using random walks. The walks impose an order and overcome the missing connectivity and structure in point cloud data.
- We introduce the shape complexity indicator function that allows to subdivide a set of shapes according to

their geometric complexity. This is particularly important because it relates to prediction confidence. A complex shape is more likely to be misclassified.

- We present an end-to-end learning framework that realizes this representation. We show that this framework works well even when the dataset has few unique objects and lacks normals. It achieves state-of-the-art results for 3D shape classification and retrieval.

## 2. Model

Given a point cloud, our goal is to learn a representation that will capture both global and local geometric information about the underlying shape, for analysis tasks. Previous works showed that learning 3D object's representation is improved by combining both local and global features [24]. As discussed above, point clouds are challenging for deep learning approaches, due to the lack of spatial structure, which prohibits the use of spatial filters on a 3D lattice. Furthermore, point clouds come in various sizes.

We propose to address these challenges by using multiple random walks through the clouds. Each walk wanders through the object and "explores" it on the way. Jointly, multiple walks provide both local shape information, as well as global shape information; the very same region can be visited multiple times from different directions. This satisfies the above desired properties since now the points have a sequential order, that covers both local and global information, and the walk length is independent w.r.t. the number of points in the cloud (up to full coverage).

Our proposed model consists of three modules, as illustrated in Figure 2: The *Random Walk Generator Module* generates multiple random walks per point set. The *Cloud-Walker Core* module extracts a single walk representation. It consists of two sub-modules: the *Point Representation Sub-module (PRM)* learns a shared, per-point representation, and the *Walk Representation sub-module (WRM)* combines the information along the walk and learns the relations between the points. Finally, the *Multi-walk Aggregation Module* produces the final shape representation, by aggregating multiple walk representations. This representation can then be used for shape analysis tasks. Hereafter we elaborate on each of these modules.

**Random walk generator.** The concept of randomness is very powerful [3, 21]. This module generates multiple random walks for a given point set. In our setup, thanks to randomness some walks explore a single region of the point set and learn its fine details alongside some broader context; While other walks cover more regions and provide the model with additional information, not seen by other walks.

A walk is a sequence of points, where each point is associated with basic local geometric information. Should the underlying surface of the point cloud existed, it would be

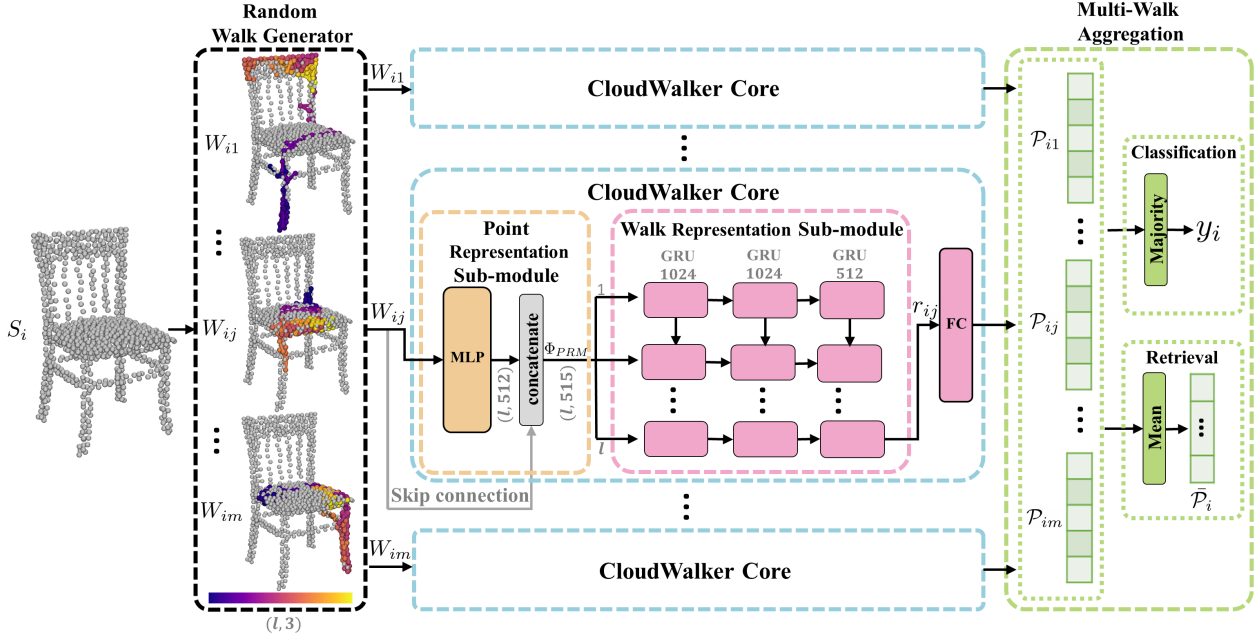


Figure 2. **CloudWalker’s pipeline.** For an input point set  $S_i$ , the *Random Walks Generator* generates several walks  $W_{ij}$ . Our model learns a representation for each walk by learning a shared, per-point representation, which are then aggregated along the walk by the *Walk Representation* sub-module. This sub-module consists of three RNN layers and produces a walk representation  $r_{ij}$ . The *Multi-Walk Aggregation* module is used at inference time to combine several walks into either the final class prediction for classification or an average representation for retrieval.

possible to utilize the adjacency information to determine, for each point, the next point on the walk. However, since connectivity information is unavailable, we propose a fast and simple approach to generate random walks.

For an input point set  $S_i$  we generate the walk  $W_{ij}$  of length  $l$  as follows. First, the walk’s origin point  $p_o \in S_i$  is randomly selected from the set. Then, points are iteratively added to the walk by selecting a random point from the set of  $k$  nearest neighbors of the last point in the sequence (excluding neighbors that were added at an earlier stage). In the rare case where all  $k$  nearest neighbors were already added to the walk, a new random un-visited point is chosen and the walk generation proceeds as before. Choosing the closest neighbor might seem like a trivial solution, however, this imposes a strong constraint on the generation process and reduces the randomness and the ability to visit sparser regions.

Since a point cloud may contain many points, an efficient nearest neighbor search is required. We propose to construct a KDtree [5] as a preprocessing step. Briefly, a KDtree is a hierarchical space-partitioning data structure, in which every node represents an axis-aligned hyper-rectangle and contains the set of points in it. This is a very efficient data structure for nearest neighbor queries. Using KDtree adds a topological challenge, moving between underlying connected components along the walk, which

works to our advantage since it allows our model to learn such crossings.

**CloudWalker Core.** Given an input walk, CloudWalker core is the main learned part of our pipeline. It is designed to learn an informative representation for a single walk. It consists of two sub-modouls, *Point Representation* sub-module and *Walk Representation* sub-module. Details for each sub-module are provided below.

**Point representation sub-module.** Given an input walk  $W_{ij}$  (the  $j^{\text{th}}$  walk for point cloud  $S_i$ ), each point  $p_t$  along the walk is embedded onto a high-dimensional feature space  $\phi_{PRM}(p_t)$ . We convert each point to a 512-dimension vector using a three layered Multi-Layer Perceptron (MLP) that shares weights across points. Then, we perform instance normalization and ReLU as nonlinear activation. We preserve the original point context by concatenating the input coordinate to the per-point representation and then feeding it into the next sub-module (WRM); see Figure 2. The module’s output is a sequence of vectors per walk,  $\Phi_{PRM}(W_{ij})$ .

**Walk representation sub-module.** The input to this stage is a sequence of high-dimensional feature vectors, a single vector for each point in the walk. The output of this module is the walk representation  $r_{ij} = \Phi_{WRM}(\Phi_{PRM}(W_{ij}))$  in the form of a single feature vector for the walk.

Similarly to [14], we use three *Gated Recurrent Units*

(GRU) [4]. Briefly, a GRU is able to "remember" and accumulate knowledge in a sequence. In our setup, each GRU layer receives all the embedded features from all points of the walk until the current point. It outputs the last hidden state, which captures an abstract representation of the input sequence. In a sense, this is the descriptor that describes the entire walk. This architecture allows walk information to persist. It is especially powerful since the local geometric detail as well as global geometric context are critical for describing the shape.

Finally, the walk representation  $r_{ij}$  is fed into a fully connected (FC) classifier to produce the prediction vector  $\widetilde{r}_{ij}$ . The number of elements in  $\widetilde{r}_{ij}$  is equal to the number of classes.

**Multi-walk aggregation module.** This module gets as input multiple walk predictions  $\widetilde{r}_{ij}, j \in [1, m]$  of a single shape  $S_i$ . To compute the probability vector we apply softmax on each walk's prediction vector:  $\mathcal{P}_{ij} = \text{softmax}(\widetilde{r}_{ij})$ .

Then, we apply a symmetric aggregation function over all of the input walks. For the symmetric function we chose the majority vote: Thus, for a given,  $S_i$  its prediction is:

$$y_i = \text{Majority}(\mathcal{C}_{i1}, \dots, \mathcal{C}_{ij}, \dots, \mathcal{C}_{im}), \quad (1)$$

where  $\mathcal{C}_{ij} = \text{argmax}(\mathcal{P}_{ij})$  is the class prediction.

We have experimented with alternative options for symmetric function, including *max* and *mean*, and found the majority vote to work best. This is attributed to its robustness to cases where the network is overconfident in a small subset of walks.

**Implementation details.** At inference, we use  $m = 48$  walks per object  $S_i$ , the length of the walk is  $l = 800$ , and  $k = 20$  nearest neighbors. In training, we use Adam optimizer with cyclic learning rate; the initial and the maximum learning rates are set to  $10^{-6}$  and  $5 \cdot 10^{-4}$  respectively. The cycle size is  $20K$  iterations and we train for a total of  $100K$  iterations. The distances between predictions and ground truth labels were minimized through cross entropy loss. Note that sometimes (e.g. ModelNet40 [34]) the shape scale is available and may be informative. In this case we add the shape's bounding box diagonal length to the representation vector and feed it to the classifier for a minor improvement. Code will be released upon acceptance.

### 3. Shape complexity indicator function

We introduce the shape complexity indicator function  $f(S_i)$ . This function, subdivides a set of shapes into two subsets: simple and complex shapes (0, 1). This is particularly important in the context of prediction confidence, since complex shapes have a higher likelihood of misclassification. Also, it enables finding out-of-distribution shapes.

To classify the shapes we propose to use two metrics that intuitively quantify the confidence in the prediction. The first metric is the cross-walk variance:

$$\text{Var}(S_i)_{cw} = \frac{1}{m} \sum_{j=1}^m |\mathcal{P}_{ij} - \text{mean}(\mathcal{P}_{ij})|^2, \quad (2)$$

here  $\mathcal{P}_{ij}$  represents the walk's probability vector and  $m$  is the number of walks used for class prediction for shape  $S_i$ . We then apply the L2 norm to get a scalar value per shape. This quantifies how much the walks agree with each other. A high value indicates that different walks predict different classes and a low value points to all walk predicting the same class. The second metric is the entropy for a single walk's prediction. For this metric we specify  $y_i$  as a one hot vector representing the class predicted by the walk. Then we calculate cross-entropy between  $y_i$  and  $\mathcal{P}_{ij}$ ,

$$CE(y_i, \mathcal{P}_{ij}) = \sum_{c=1}^{\#classes} (y_i)_c \cdot \log((\mathcal{P}_{ij})_c). \quad (3)$$

This metric intuitively quantifies the informativeness of each walk. A low value means that it is close to a Kronecker delta function for the desired class and a high value indicates similarity to other classes.

The indicator function is then computed as the linear function, above which the number of shapes that were classified correctly and incorrectly (in the training set) are approximately equal.

$$f(S_i) = \begin{cases} 1 & \text{Var}(S_i)_{cw} > a \cdot CE(y_i, \mathcal{P}_{ij}) + b \\ 0 & \text{otherwise} \end{cases} \quad (4)$$

Here,  $a$  and  $b$  are the line parameters.

Figure 3 presents some examples of shapes in the complex subset according to the proposed indicator function. It shows that most of these shapes are out of distribution and can be easily misclassified by a human when appearing out of context e.g. the human is wearing a wizard costume and is actually only a silhouette (points are on a 2D plane), the sink includes shelves and a counter, and the toilet has a vase or cup-like geometric features. Additional information and empirical results for the shape complexity indicator function is provided in the supplemental material.

## 4. Applications

We evaluate the performance of our model on two main tasks: 3D shape classification and 3D object retrieval.

### 4.1. 3D shape Classification

Given a 3D point set, the goal is to classify it into one of pre-defined classes. Our model outputs a classification prediction probability vector for each walk. At inference, a

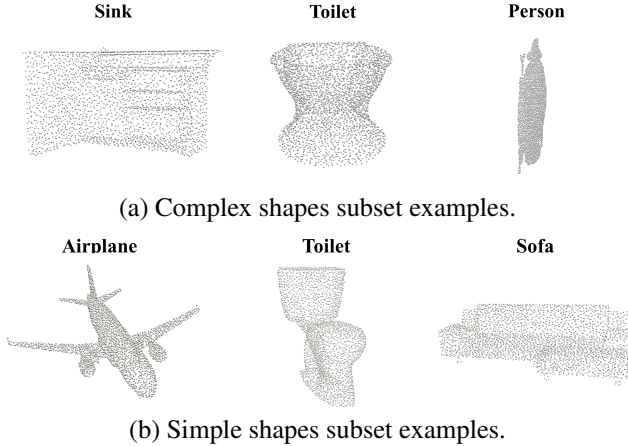


Figure 3. **Shape complexity indicator function results.** Visualizing complex and simple 3D objects from ModelNet40 [34] as determined by the proposed indicator function. It shows unique object and out-of-distribution geometry for the complex subset and standard average shapes for the simple subset.

majority prediction of the walks’ prediction vectors is calculated to produce the final result.

**Evaluation measures.** For each dataset we report both *instance accuracy (IA)* and *class accuracy (CA)*. Instance accuracy is defined as the percentage of the correctly-classified objects,

$$IA = \frac{\#correctly\_classified}{\#test\_instances} \quad (5)$$

Class accuracy is the mean of per-class instance accuracy,

$$CA = \frac{1}{C} \sum_{i \in C} IA(i), \quad (6)$$

where  $C$  is the number of classes.

**Datasets.** We present our results on three commonly-used datasets, where each contains different types of objects, different numbers of classes, a different number of objects per class and different challenges. Figure 4 presents some examples from the datasets.

*3D-FUTURE* [9] is a recent dataset that contains 9,992 industrial CAD models of furniture. It consists of 7 super-categories, with 1-12 sub-categories each, for a total of 34 categories. The train/test split is 6,699/3,293. This dataset is challenging both due to the objects it contains and due to its hierarchical structure, as objects in the same category but different sub-categories may resemble each other, requiring fine-grained information in the shape representation.

*ScanObjectNN* [31] is a real-world dataset that contains 2902 unique object scans from 15 classes. The objects are corrupted in various ways to create a set of  $\sim 15k$  objects

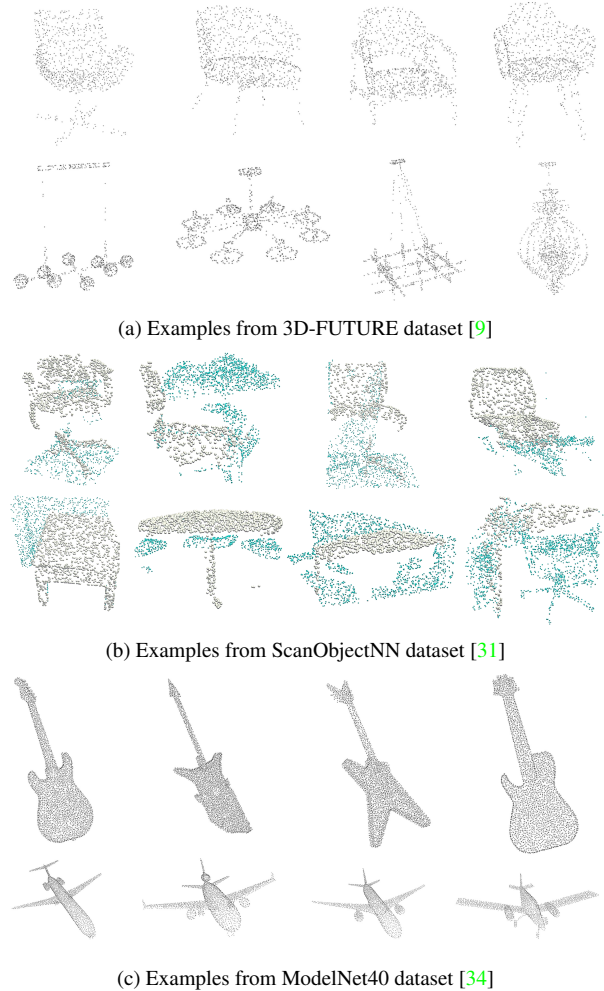


Figure 4. **Datasets snapshot.** Datasets vary in density, noise and available classes. Presented here are typical objects from (a) 3D-FUTURE [9] which contains uniformly sampled industrial CAD models (chair and lamp classes), (b) ScanObjectNN [31] which contains real-world objects, with their background in cyan (chair and table classes), and (c) ModelNet40 [34] which contains CAD models (guitar and airplane classes).

that are used for training and testing. In terms of the training and test sets, we follow the official data split in [31]. This dataset is highly challenging due to the various types of data corruptions found in scans which include: background points, object partiality, and different transformation variants (translation, rotation, and scale). We performed our experiment on the most challenging variant of the dataset, *PB T50 RS*, with and without background points.

*ModelNet40* [34] contains clean CAD models. There are 12,311 meshes divided into 40 classes, with 9,843 shapes for training and 2,468 for testing. Corresponding point clouds are generated by uniformly sampling, following the sampling protocol of [24].

Method	Input	IA (%)	CA (%)
MVCNN [29]	Multi-views	69.2	65.4
PointNet++ [24]	Point cloud	69.9	66.0
Ours	Point cloud	<b>70.6</b>	<b>67.8</b>

Table 1. **Classification results on 3D-FUTURE dataset.** Our results outperform those reported in [9] using both multi-view and point clouds as input. We note PointNet++ uses normals while we use only the points.

Category	Ours	PointNet++	MVCNN
Dining Chair	<b>76.8</b>	63.9	50.5
Lounge/Office Chair	54.0	<b>60.5</b>	60.3
Classic Chinese Chair	<b>62.5</b>	<b>62.5</b>	57.1
Barstool	<b>88.8</b>	66.7	32.0

Table 2. **Classification results on 3D-FUTURE [9]** for the *Chair* super-category (Instance Accuracy %) compared to PointNet++ [24] and MVCNN [29].

**Quantitative results.** The results for 3D-FUTURE [9] are presented in Table 1. It shows that our method outperforms not only previous point-based, but also multi-view methods, reported for this dataset. We followed the same training protocol for point-based methods as specified by Fu *et al.* [9] and trained our model with 1K points per object. In particular, we uniformly sampled 1024 points for each shape. Our results outperform the others in both IA and CA evaluation measures.

Table 2 presents a zoom-in to the super-category *Chair*. It shows how challenging this dataset is because of its similar sub-categories. A full comparison of all categories is available in the supplementary material. We note that while [24] uses normals as additional information, we do not. The mere vertices locations suffice for our method. This is especially important in cases where normals are unavailable, as normals are not outputs of mist scanners and normal estimation is possible, but is not a trivial problem [1, 10, 16]. After all, normal estimation is "almost" surface reconstruction, and the reconstruction of a surface is exactly what we wish to avoid.

For ScanObjectNN, Table 3 presents the results with and without background points of real-world scans. It shows that the overall accuracy is better compared to state of the art methods [31]. When trained and tested without the background points, our average class accuracy 78.5% is higher than all reported results while maintaining competitiveness on the overall accuracy.

Table 4 reports the results on the ModelNet40 [34] dataset. For this dataset we achieved competitive results. ModelNet40 is known to be a difficult and saturated dataset, partially because of cross-labeled classes

Methods	w/o BG (%)		w/ BG (%)	
	IA	CA	IA	CA
3DmFV [2]	69.8	-	63.0	58.1
PointNet [23]	74.4	-	68.2	63.4
SpiderCNN [36]	76.9	-	73.7	69.8
PointNet++ [24]	80.2	-	77.9	75.4
DGCNN [32]	<u>81.5</u>	-	78.1	73.6
PointCNN [17]	80.8	-	78.5	75.1
DRNet [25]	-	-	<u>80.3</u>	<u>78.0</u>
GBNet [26]	-	-	<b>80.5</b>	77.8
BGA-PN++ [31]	-	-	80.2	77.5
BGA-DGCNN [31]	-	-	79.7	75.7
Ours	<b>82.2</b>	79.5	<u>80.3</u>	<b>78.5</b>

Table 3. **Classification results on ScanObjectNN [31].** We use the difficult variant of the dataset, PB T50 RS, with (w/) and without (w/o) background (BG) points. We achieve SOTA results on the variant without the background; (CA results were not reported for objects without background.) we achieve CA SOTA results on the variant with the background and competitive IA results. The second best is underlined.

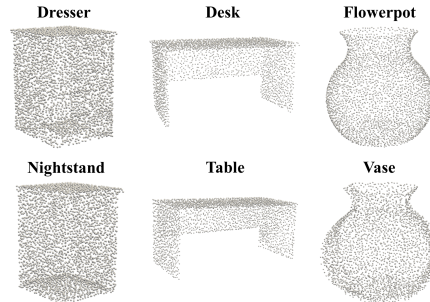


Figure 5. **ModelNet40 [34] difficult examples.** Objects from different classes have similar geometric properties.

(desk/table, plant/flower-pot/vase, night-stand/dresser), as illustrated in Figure 5.

We report that when we choose the second best prediction for the mis-classified objects in ModelNet40 dataset, 97% of the test instances are correctly classified. Similarly, for the 3DFuture dataset we get 89% accuracy (~ 19% improvement). This finding further shows that some categories have fine-grained differences that are difficult to discriminate.

## 4.2. Retrieval

Given a query object, the goal is to retrieve objects from the dataset, ordered by their relevancy (similarity) to the query. There are various ways to evaluate shape retrieval. The most common evaluation is the *mean Average Preci-*

Method	IA (%)	CA (%)
PointTrans. [38]	93.7	90.6
PointCNN [17]	92.2	88.1
PointNet [23]	89.2	86
PointNet++ [24]	90.7	-
KPConv [30]	92.9	-
SpiderCNN [36]	92.4	-
CurveNet [35]	<b>93.8</b>	-
GBNet [26]	<b>93.8</b>	<b>91</b>
Ours	92.8	89.6

Table 4. **Classification results on ModelNet40 [34]** For this dataset we are show competitive results.

sion ( $mAP$ ) over test queries:

$$mAP = \frac{1}{Q} \sum_{i=1}^Q AP(S_i), \quad (7)$$

where  $Q$  is the number of queries in the set.  $AP$  is defined as  $AP = \frac{1}{GTP} \sum_k^N P@k \times rel@k$ , where  $GTP$  is the number of ground truth positives,  $N$  is the size of the ordered set,  $P@k$  refers to the precision at  $k$  and  $rel@k$  is an indicator function which equals 1 if the object at rank  $k$  is from the same class as query  $S_i$  and 0 otherwise.

We present our results on commonly used datasets for shape retrieval task, ModelNet40 and ModelNet10 [34]. We use the most common train/test splits: 9,843/2,468 for ModelNet40 and 3,991/908 for ModelNet10. We used the output feature vector from our classification network by averaging all walks probability vectors for each object and get a global shape feature vector  $\bar{P}_i$ ; see Figure 2.

Table 5 shows that our method achieves SOTA results on both ModelNet40 and ModelNet10 [34]. It outperforms approaches that use a variety of 3D representations, including, meshes, multi-views, and point clouds.

Figure 6 presents qualitative results for object retrieval on ModelNet40 [34] dataset. It shows the top five retrieved objects by our model. As can be seen, the retrieved objects are indeed similar and thus belong to the same class. In the bottom row we show a particularly interesting case where the query object belongs to the *plants* category, but the highlighted model belongs to a different category and thus considered to be an error. However, this is in fact the exact same object with different set of points. This example demonstrates some of the challenges in the dataset.

## 5. Ablation study

**Walk length.** In this experiment we explore the effects of walk length, *i.e.* the number of points in each walk, on the performance of classification. Table 6 shows that a longer walk improves performance up to a certain length. This can

Method	input	ModelNet40	ModelNet10
GWCNN [6]	Mesh	59.0	74.0
MeshNet [7]	Mesh	81.9	-
MVCNN [29]	MV	79.5	-
SeqViews [12]	MV	89.1	-
PointNet [23]	PC	70.5	-
PointCNN [17]	PC	83.8	-
DGCNN [32]	PC	85.3	-
DensePoint [18]	PC	88.5	93.2
Ours	PC	<b>92.9</b>	<b>93.7</b>

Table 5. **3D Shape Retrieval results.** This table shows the  $mAP$  on ModelNet40 & ModelNet10 [34], sorted by the input type (Point Clouds, Multi-views, and meshes). The proposed CloudWalker outperforms other methods.

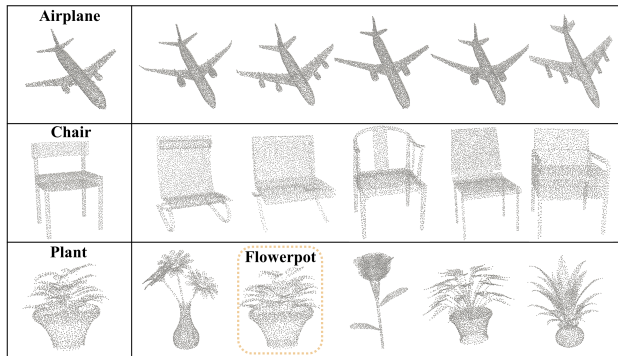


Figure 6. **Qualitative results for Object Retrieval.** The query test objects are on the left, where the top five retrieved objects are on the right. The falsely retrieved object is highlighted.

Walk length	IA (%)	CA (%)
0.1V	75.3	72.1
0.2V	78.0	75.2
0.4V	<b>82.2</b>	<b>79.5</b>
0.5V	79.3	76.4

Table 6. **Walk length ablation.** Performance improves as length increases, up to a certain length. Tested on ScanObjectNN [31].

be explained by the fact that longer walks are likely to have better coverage of the object, and thus better distinguish between different categories. However, when the walk is too long, the GRUs’ ability to “remember” points in the sequences is reduced, which negatively impacts performance. For example, on ScanObjectNN [31], we get improvement when using up to 40% of the total number of vertices per walk. This quantity is dataset dependant, however we found 40% to perform well across multiple datasets.

**Aggregation method.** In our model, we aggregate predic-

Aggregation method	IA (%)	CA (%)
Average	92.7	89.5
Max	92.5	89.4
Majority	<b>92.8</b>	<b>89.6</b>

Table 7. **Aggregation method ablation.** Majority voting is slightly better than the alternative symmetric functions. Tested on ModelNet40 [34].

Number of walks	IA (%)	CA (%)
4	68.6	65.5
16	69.7	67.1
32	69.8	67.5
48	<b>70.6</b>	<b>67.8</b>
64	<u>70.5</u>	67.5
96	70.3	<b>67.9</b>

Table 8. **Number of walks ablation.** The accuracy improves with the number of walks per shape. Tested on 3D-FUTURE [9].

tions from multiple walks on the shape. Table 7 compares three symmetric aggregation functions. While the results are similar, there is a slight advantage to majority voting.

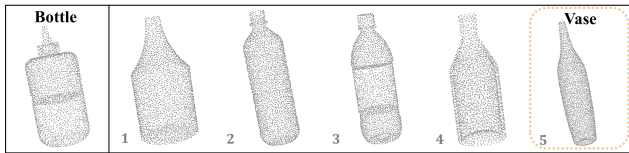
**Number of walks.** We study how the number of walks used at inference influences classification accuracy. Table 8 shows that as the number of walks increases, the accuracy improves up to 48 walks where it saturates. Note that, even very few walks result in very good accuracy. This means that the number of walks may be a tuneable parameter that balances the tradeoff between computational power and accuracy. In our method, we chose to use 48 walks.

**Random walk generation method.** Generating random walks can be performed in various ways. In the following we explore several options, in all of which the first point is randomly chosen and the next points are sequentially added from the last point’s neighbors. The options are: (1) Random—randomly choosing among the point’s unvisited neighbors with a uniform distribution. (2) High variance—calculating the change in variance for each neighbor of the most recently added point and selecting the one that increases the variance the most. (3) Combined—combining both random and high variance methods by choosing a neighbor who increases the variance 30% of the times and randomly otherwise. Note that the heuristic based on the walk variance is effective, but it is not sufficient since it reduces randomness. The results are presented in Table 9. We found that the random strategy is the best, reinforcing our claim of the power of randomness.

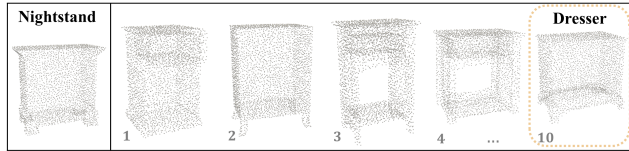
**Limitations.** Figure 7 shows failure cases in the retrieval task. In (a), the 5<sup>th</sup> retrieved object is a vase, rather than a bottle. This vase is geometrically similar to a bottle, how-

Generation method	IA (%)	CA (%)
Random	<b>92.8</b>	<b>89.6</b>
High variance	90.2	86.5
Combined	91.7	87.9

Table 9. **Walk generation ablation.** Random walk generation performs better than hand-crafted heuristics. Tested on ModelNet40 [34].



(a) Same geometry with a different small detail (top cap).



(b) Geometrically similar objects are in different categories.

Figure 7. **Limitation.** When objects are geometrically similar, yet belong to different classes, our method might err.

ever the top differs. Most of the walks provide the geometry of a vase. There is a lower probability of capturing this particular geometry which distinguishes it from a bottle due to the few points in that region. In (b) we present five of the top ten objects retrieved for the leftmost nightstand. A dresser is placed at the 10th spot. These objects belong to different classes but have similar geometry.

**Negative societal potential impact.** Many downstream applications may be enabled by the proposed representation and may be leveraged for positive and negative outcomes. For example, CloudWalker may be extended to generative tasks with potential misuses including mechanical design unauthorized reproduction. Furthermore, walk-based adversarial attacks that may be misused in the context of autonomous driving. Note that, while possible, these extensions are unlikely and require additional work.

## 6. Conclusion

This paper introduces a novel approach for representing point clouds suited for deep learning architectures. The key idea is to represent the point cloud using multiple random walks on the shape. We utilize this representation and introduce CloudWalker, an end-to-end shape representation learning pipeline. The approach is general, yet simple, and relies on the power of randomness. We have shown our approach to be very effective for the tasks of classification and retrieval. Furthermore, we proposed a shape complexity in-



indicator function, which leverages random walks. It lets us divide 3D datasets into simple and complex subsets.

An interesting avenue for future work may explore extending the shape complexity function to higher order polynomials or an implicit function rather than the linear function we use now. Additionally, alternative random walk generation processes and their use in other tasks is another path to explore.

## References

- [1] Yizhak Ben-Shabat and Stephen Gould. Deepfit: 3d surface fitting via neural network weighted least squares. In *ECCV*, pages 20–34. Springer, 2020. 2, 6
- [2] Yizhak Ben-Shabat, Michael Lindenbaum, and Anath Fischer. 3DMFV: Three-dimensional point cloud classification in real-time using convolutional neural networks. 3:3145–3152, 2018. 2, 6
- [3] Bernard Chazelle. *The discrepancy method: randomness and complexity*. Cambridge University Press, 2001. 2
- [4] Kyunghyun Cho, Bart Van Merriënboer, Caglar Gulcehre, Dzmitry Bahdanau, Fethi Bougares, Holger Schwenk, and Yoshua Bengio. Learning phrase representations using RNN encoder-decoder for statistical machine translation. *arXiv preprint arXiv:1406.1078*, 2014. 4
- [5] Mark De Berg, Marc Van Kreveld, Mark Overmars, and Otfried Schwarzkopf. Computational geometry. In *Computational geometry*, pages 1–17. Springer, 1997. 3
- [6] Danielle Ezuz, Justin Solomon, Vladimir G Kim, and Mirela Ben-Chen. GWCNN: A metric alignment layer for deep shape analysis. In *Computer Graphics Forum*, volume 36, pages 49–57. Wiley Online Library, 2017. 7
- [7] Yutong Feng, Yifan Feng, Haoxuan You, Xibin Zhao, and Yue Gao. Meshnet: Mesh neural network for 3d shape representation. In *AAAI*, volume 33, pages 8279–8286, 2019. 7
- [8] David Forsyth and Jean Ponce. *Computer vision: A modern approach*. Prentice hall, 2011. 1
- [9] Huan Fu, Rongfei Jia, Lin Gao, Mingming Gong, Binqiang Zhao, Steve Maybank, and Dacheng Tao. 3d-future: 3d furniture shape with texture. *IJCV*, pages 1–25, 2021. 2, 5, 6, 8
- [10] Paul Guerrero, Yanir Kleiman, Maks Ovsjanikov, and Niloy J Mitra. Pcpnet learning local shape properties from raw point clouds. In *Computer Graphics Forum*, volume 37, pages 75–85. Wiley Online Library, 2018. 2, 6
- [11] Yulan Guo, Hanyun Wang, Qingyong Hu, Hao Liu, Li Liu, and Mohammed Bennamoun. Deep learning for 3d point clouds: A survey. *IEEE TPAMI*, 2020. 1
- [12] Zhizhong Han, Mingyang Shang, Zhenbao Liu, Chi-Man Vong, Yu-Shen Liu, Matthias Zwicker, Junwei Han, and CL Philip Chen. SeqViews2SeqLabels: Learning 3d global features via aggregating sequential views by rnn with attention. *IEEE Transactions on Image Processing*, 28:658–672, 2018. 7
- [13] Roman Klokov and Victor Lempitsky. Escape from cells: Deep kd-networks for the recognition of 3d point cloud models. In *ICCV*, pages 863–872, 2017. 2
- [14] Alon Lahav and Ayellet Tal. MeshWalker: Deep mesh understanding by random walks. *ACM TOG*, 39:1–13, 2020. 2, 3
- [15] Huan Lei, Naveed Akhtar, and Ajmal Mian. Octree guided cnn with spherical kernels for 3d point clouds. In *CVPR*, pages 9631–9640, 2019. 2
- [16] Jan Eric Lenssen, Christian Osendorfer, and Jonathan Masci. Deep iterative surface normal estimation. In *CVPR*, pages 11247–11256, 2020. 2, 6
- [17] Yangyan Li, Rui Bu, Mingchao Sun, Wei Wu, Xinhan Di, and Baoquan Chen. PointCNN: Convolution on x-transformed points. *Advances in Neural Information Processing Systems (NeurIPS)*, 31:820–830, 2018. 2, 6, 7
- [18] Yongcheng Liu, Bin Fan, Gaofeng Meng, Jiwen Lu, Shiming Xiang, and Chunhong Pan. Densepoint: Learning densely contextual representation for efficient point cloud processing. In *ICCV*, pages 5239–5248, 2019. 2, 7
- [19] Yongcheng Liu, Bin Fan, Shiming Xiang, and Chunhong Pan. Relation-shape convolutional neural network for point cloud analysis. In *CVPR*, pages 8895–8904, 2019. 2
- [20] Steve Marschner and Peter Shirley. *Fundamentals of computer graphics*. CRC Press, 2018. 1
- [21] Rajeev Motwani and Prabhakar Raghavan. *Randomized algorithms*. Cambridge university press, 1995. 2
- [22] Giannis Nikolentzos and Michalis Vazirgiannis. Random walk graph neural networks. *Advances in Neural Information Processing Systems (NeurIPS)*, 33:16211–16222, 2020. 2
- [23] Charles R Qi, Hao Su, Kaichun Mo, and Leonidas J Guibas. Pointnet: Deep learning on point sets for 3d classification and segmentation. In *CVPR*, pages 652–660, 2017. 1, 2, 6, 7
- [24] Charles Ruizhongtai Qi, Li Yi, Hao Su, and Leonidas J Guibas. Pointnet++: Deep hierarchical feature learning on point sets in a metric space. 30, 2017. 1, 2, 5, 6, 7
- [25] Shi Qiu, Saeed Anwar, and Nick Barnes. Dense-resolution network for point cloud classification and segmentation. In *Proc. of the IEEE Winter Conference on Applications of Computer Vision (WACV)*, pages 3813–3822, 2021. 6
- [26] Shi Qiu, Saeed Anwar, and Nick Barnes. Geometric back-projection network for point cloud classification. *IEEE Transactions on Multimedia*, 2021. 6, 7
- [27] Yongming Rao, Jiwen Lu, and Jie Zhou. Spherical fractal convolutional neural networks for point cloud recognition. In *CVPR*, pages 452–460, 2019. 2
- [28] Martin Simonovsky and Nikos Komodakis. Dynamic edge-conditioned filters in convolutional neural networks on graphs. In *CVPR*, pages 3693–3702, 2017. 2
- [29] Hang Su, Subhransu Maji, Evangelos Kalogerakis, and Erik Learned-Miller. Multi-view convolutional neural networks for 3d shape recognition. In *ICCV*, pages 945–953, 2015. 6, 7
- [30] Hugues Thomas, Charles R Qi, Jean-Emmanuel Deschaud, Beatriz Marcotegui, François Goulette, and Leonidas J Guibas. Kpconv: Flexible and deformable convolution for point clouds. In *ICCV*, pages 6411–6420, 2019. 2, 7
- [31] Mikaela Angelina Uy, Quang-Hieu Pham, Binh-Son Hua, Duc Thanh Nguyen, and Sai-Kit Yeung. Revisiting point

- cloud classification: A new benchmark dataset and classification model on real-world data. In *ICCV*, 2019. 2, 5, 6, 7
- [32] Yue Wang, Yongbin Sun, Ziwei Liu, Sanjay E Sarma, Michael M Bronstein, and Justin M Solomon. Dynamic graph cnn for learning on point clouds. *Acm Transactions On Graphics (tog)*, 38:1–12, 2019. 6, 7
- [33] Wenxuan Wu, Zhongang Qi, and Li Fuxin. Pointconv: Deep convolutional networks on 3d point clouds. In *CVPR*, pages 9621–9630, 2019. 2
- [34] Zhirong Wu, Shuran Song, Aditya Khosla, Fisher Yu, Linguang Zhang, Xiaoou Tang, and Jianxiong Xiao. 3d shapenets: A deep representation for volumetric shapes. In *CVPR*, pages 1912–1920, 2015. 2, 4, 5, 6, 7, 8
- [35] Tiange Xiang, Chaoyi Zhang, Yang Song, Jianhui Yu, and Weidong Cai. Walk in the cloud: Learning curves for point clouds shape analysis. In *ICCV*, 2021. 2, 7
- [36] Yifan Xu, Tianqi Fan, Mingye Xu, Long Zeng, and Yu Qiao. Spidercnn: Deep learning on point sets with parameterized convolutional filters. In *ECCV*, pages 87–102, 2018. 2, 6, 7
- [37] Manzil Zaheer, Satwik Kottur, Siamak Ravanbakhsh, Barnabas Poczos, Russ R Salakhutdinov, and Alexander J Smola. Deep sets. 2017. 1
- [38] Hengshuang Zhao, Li Jiang, Jiaya Jia, Philip HS Torr, and Vladlen Koltun. Point transformer. pages 16259–16268, 2021. 7

# CloudWalker: 3D Point Cloud Learning by Random Walks for Shape Analysis— Supplementary Material

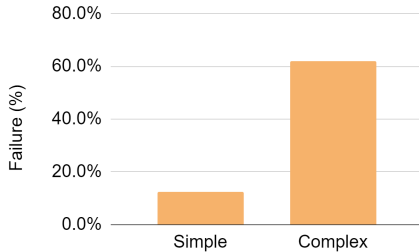


Figure 8. **User study quantitative results.** On the complex subset, the majority of participants (~ 62%) chose a different option than the ground truth.

## 7. Shape complexity indicator function

Recall that our shape complexity indicator function,  $f(S_i)$ , subdivides a set of shapes into two subsets: simple and complex shapes. The perceived classification complexity or simplicity of an object is difficult to quantify and is often subjective. Therefore, we verify the function subdivision using a user study.

In the study we present participants with 3D objects from ModelNet40 dataset and ask them to choose whether the shape belongs to (1) ground truth category, (2) prediction category (if different), (3) second best category (if exists), (4) can't decide or, (5) none of the above options.

For each participant, 95 objects were randomly selected from the complex and simple shapes subsets (total of 190 shapes per participant). Participants were allowed to answer only a subset of the questions. In total, each question was answered by an average of 72 participants and there were 92 participated in the user study. The study has an approximate 1:1 male:female ratio in the age range of 20 and 60, with at least a high school education. Note that prior to presenting the questions to participants, several typical objects from each category (from the training set) were presented to them. Also note that if the prediction/second best is the ground truth we randomly choose a category.

The study results are presented in Figure 8. It shows that, as we expected, for the simple objects, the percentage of incorrect answers is low 12.5% , while for the complex ones, it is much higher 62.1%. Note that we expected a moderate level of success even in the complex models since the geometry of some shapes is non-standard and out-of-distribution but are likely to be recognized by a human as shown in Figure 9.

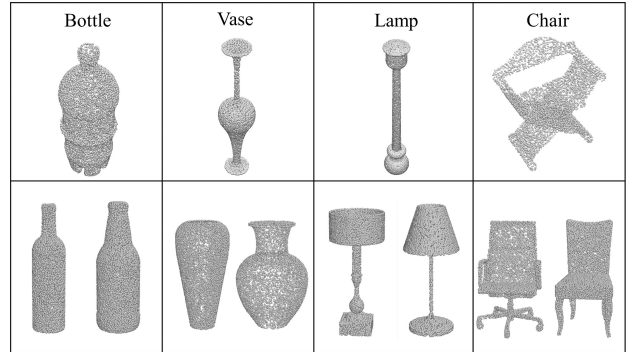


Figure 9. **Objects from the complex (top) and simple (bottom) subsets.** The top row shapes are easy to classify by a human but are out-of-distribution compared to other shapes in their category in the bottom row.

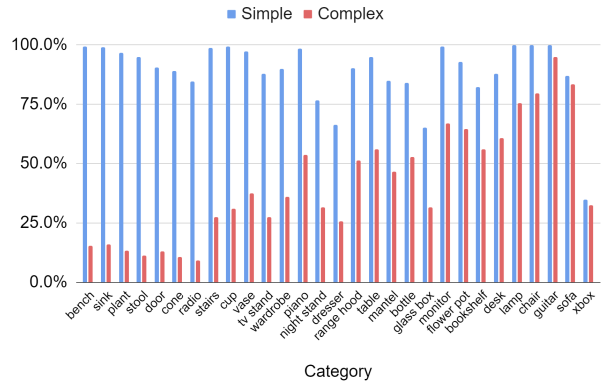


Figure 10. **User study results per category.** Percentage of correct answers for each category. The *simple* bar is significantly higher than the *complex* bar. The right side displays both hard-identified objects for both groups and recognizable objects despite their geometric complexity.

Figure 10 displays quantitative results for each category, sorted by simple/complex ratio. Each bar describes the percentage of success on the objects from the simple or complex subsets. Overall, the bar for complex objects is significantly lower than the bar for simple objects as we expected.

Category	Ours	PointNet++	MVCNN
Children Cabinet	16.0%	32.1%	<b>72.0%</b>
Nightstand	<b>83.5%</b>	71.8%	75.0%
Bookcase	58.7%	52.3%	<b>66.7%</b>
Wardrobe	<b>85.0%</b>	82.0%	56.7%
Coffee Table	<b>83.7%</b>	82.6%	67.9%
Corner/Side Table	73.0%	<b>74.7%</b>	64.5%
Side Cabinet	<b>69.5%</b>	65.2%	47.9%
Wine Cabinet	44.3%	<b>67.1%</b>	62.9%
TV Stand	<b>80.5%</b>	73.6%	73.5%
Drawer Chest	44.8%	55.2%	<b>67.5%</b>
Shelf	48.4%	48.4%	<b>51.9%</b>
Round End Table	<b>93.7%</b>	75.0%	52.2%
King-size Bed	89.6%	<b>91.2%</b>	78.6%
Bunk Bed	<b>88.8%</b>	77.8%	57.1%
Bed Frame	<b>95.4%</b>	93.8%	93.8%
Single bed	<b>68.9%</b>	<b>68.9%</b>	67.7%
Kids Bed	00.0%	<b>14.3%</b>	12.5%
Dining Chair	<b>76.8%</b>	63.9%	50.5%
Lounge/Office Chair	54.0%	<b>60.5%</b>	60.3%
Classic Chinese Chair	<b>62.5%</b>	<b>62.5%</b>	57.1%
Barstool	<b>88.8%</b>	66.7%	32.0%
Dressing Table	<b>77.3%</b>	68.2%	73.7%
Dining Table	76.0%	61.1%	<b>84.8%</b>
Desk	30.9%	20.4%	<b>54.0%</b>
Three-seat Sofa	<b>83.1%</b>	82.6%	71.7%
armchair	<b>74.9%</b>	68.0%	72.5%
Loveseat Sofa	45.5%	<b>64.5%</b>	62.9%
L-shaped Sofa	<b>92.9%</b>	85.9%	83.3%
Lazy Sofa	42.8%	50.0%	<b>66.7%</b>
Stool	70.9%	75.8%	<b>91.9%</b>
Pendant Lamp	<b>92.8%</b>	90.9%	89.8%
Ceiling Lamp	<b>72.0%</b>	70.7%	63.0%
Average Class Accuracy	<b>67.8%</b>	66.0%	65.2%
Instance Accuracy	<b>70.6%</b>	69.9%	69.2%

Table 10. **Classification results for each category of 3D-FUTURE.** We note PointNet++ uses normals and Multi-scale grouping (MSG) and we do not, while we use only the points. MVCNN uses 12 view + ResNet50 backbone.

## 8. Classification additional results

Table 10 presents quantitative result for classification on 3D-FUTURE for each category. It shows that our method outperforms both, point-based and multi-view methods reported for this dataset. Our model leads in 18/32 categories.